gives a ratio for the red film before contraction approximately four times that for the blue one (30 and 7 percent, respectively).

The concentration of the merocyanine molecules in the blue fluid films is determined by the thermal spiropyran-merocyanine equilibrium. Irradiation of these films at temperatures higher than 85°C does not increase the concentration of the merocyanine molecules, because of the fast thermal back reaction (*1*). The low concentration of merocyanine makes formation of stacks improbable.

On the other hand, high concentrations of merocyanines and H-stacks are formed on irradiation and slow heating of a film from room temperature. This is probably determined by two factors: (i) the lower rate of thermal conversion of merocyanine to spiropyran at the lower temperature and (ii) the retardation of this reaction due to the organization of the merocyanines in the stacks. Very significant stabilization of transient merocyanines in H-stacks has been demonstrated in our recent studies (*6, 14, 15*). The thermal conversion of the stacked merocyanines to spiropyrans proceeds only at the ends of the stacks.

We believe that the red melt is a complex liquid system in which there are present spiropyran molecules, H-stacks, and separated merocyanine molecules, all interconvertible to one another (Fig. 2). Irradiation of this melt leads to an increase in the concentration of separated merocyanine molecules, and these have a good chance of joining the H-stacks already formed on irradiation at low temperature. This growth of the stacks inhibits the thermal back-conversion to spiropyran. Formation of the high-density stacks from loosely arranged bulky spiropyran molecules must lead to contraction of the fluid. The healing of the holes in the dark is determined by the tendency of the fluid to acquire a minimum surface and by the expansion of the films. The expansion is connected, apparently, with destruction of large stacks due to the thermal merocyanine-spiropyran conversion. Both photocontraction and the thermal expansion are controlled by processes occurring at the stack ends. Therefore, the rates of both the direct and back reactions are inversely proportional to the length of the stacks at a given merocyanine/spiropyran ratio. Long irradiation should bring about the accumulation of long stacks at the expense of short ones. This may provide an explanation for the decay of the effect on repetitive contraction-expansion cycles. Growth of the stack length must increase melt viscosity, which may also contribute to the decay of the photocontraction.

The x-ray diffraction patterns of the cooled red and blue melts show that in both cases we are dealing with noncrystalline materials. The patterns do not allow us to decide unambiguously whether **2a** preserves some remnant order after melting. The order, if any, must be poorer than in liquid crystals. Even in the case of liquid crystals, the x-ray diffraction patterns are not always distinguishable from those of the isotropic phases (*16*).

Substitution of the mesogenic group in spiropyrans **1** by other groups [$-C_6H_{12}OH$,$-C_6H_{12}OCOC(CH_3) = CH_2$] and even slight modification of the mesogenic group (methoxy instead of cyano group) lead to disappearance of the photocontraction effect. This points to the importance of this moiety. Further, a value of $d \sim 5$ Å, deduced from the halo in the x-ray pattern, is typical of the intermolecular distance in nematics having molecular structures similar to that of our mesogenic group (*16*). One may assume that mesogenic groups provide head-to-head positioning of the spiropyran moieties, which facilitates formation of merocyanine stacks (Fig. 2).

An interesting feature of the photocontraction is the formation of holes inside the film, with no decrease or a slight increase of the perimeter. The light that converts spiropyran to merocyanine penetrates only a very thin layer of the film (for example, the absorbance of a red film 10 μm thick is more than 10). Therefore, in order to achieve high conversions of spiropyran to merocyanine, there must occur some sort of convective flow that allows exposure to light of the material originally in the lower layers, leading to the formation of holes inside the film.

The suggested mechanism is a preliminary attempt to explain an astonishing phenomenon, the marked contraction of a liquid on illumination with light. Such an effect will occur only in a system having very special microstructure, which may appropriately be termed a "quasi-liquid."

IVAN CABRERA
FELIX SHVARTSMAN
OLGA VEINBERG
VALERI KRONGAUZ
Department of Structural Chemistry, Weizmann Institute of Science, Rehovot, 76100, Israel

References and Notes

1. R. C. Bertelson, *Photochromism*, G. Brown, Ed. (Wiley, New York, 1971), chap. 3.
2. V. A. Krongauz and E. S. Goldburt, *Nature (London)* **271**, 435 (1978).
3. V. A. Krongauz, S. N. Fishman, E. S. Goldburt, *J. Phys. Chem.* **82**, 2469 (1978).
4. G. R. Meredith, V. Krongauz, D. J. W. Williams, *Chem. Phys. Lett.* **87**, 289 (1982).
5. V. A. Krongauz and E. S. Goldburt, *Macromolecules* **14**, 1382 (1981).
6. E. Goldburt *et al.*, *ibid.*, in press.
7. D. M. Sturmer and D. W. Heseltine, *The Theory of the Photographic Process*, H. Jammes, Ed. (Macmillan, New York, 1977), chaps. 7 and 8.
8. F. Shvartsman and V. Krongauz, *Nature (London)* **309**, 608 (1984).
9. P. Duvette and T. Y. Shen. *Carbohydr. Res.* **83** (No. 1), 178 (1980).
10. E. Zaitseva *et al.*, *Chem. Heterocycl. Compd.* **10**, 1362 (1973).
11. C. Cavallito and J. Buck, *J. Am. Chem. Soc.* **65**, 2140 (1943).
12. A. Hassner and V. Alexanian, *Tetrahedron Lett.* **46**, 4475 (1978).
13. S. Clark, M. Kahn, A. Mitra, *J. Org. Chem.* **43**, 2923 (1978).
14. E. Goldburt, F. Shvartsman, V. Krongauz, *Macromolecules* **17**, 1225 (1984).
15. E. Goldburt and V. Krongauz, in preparation.
16. H. Kelker and R. Hatz, *Handbook of Liquid Crystals* (Verlag Chemie, Deerfield Beach, Fla., 1980), chap. 5.
17. We thank M. D. Cohen and E. Fischer for valuable comments on the manuscript.

15 March 1984; accepted 18 July 1984

Temporal Variability of the Antarctic Circumpolar Current Observed from Satellite Altimetry

Abstract. *Sea level measurements by the Seasat altimeter were used to study the temporal variability of the Antarctic Circumpolar Current between July and October 1978. Large-scale zonal coherence in the cross-stream sea level difference was observed, indicating a general increase in the surface geostrophic velocity of the current around the Southern Ocean. The result demonstrates the power of satellite altimetry to monitor the variability of large-scale ocean currents.*

Recent observations (*1, 2*) have revealed that there are substantial temporal variations in the mass transport of the Antarctic Circumpolar Current (ACC). The magnitude of the variation (peak-to-peak range) has been estimated to be 40 sverdrups (1 Sv = 10^9 kg/sec), about 30 percent of the mean transport. ACC transport variations of this magnitude have profound effects on the circulation of the world's oceans, which are important determinants of the global climate (*3*).

Because synoptic global observations of the ACC are lacking, very little is known about the spatial structure of its temporal variability. For example, what is the zonal scale of the variability? Does

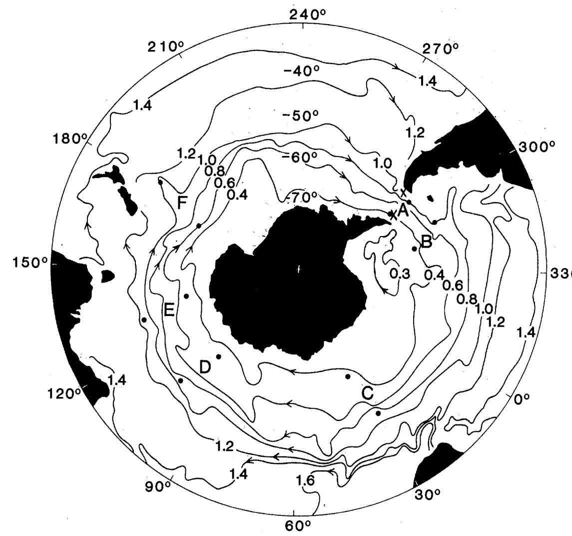

Fig. 1. Long-term averaged sea-surface dynamic topography of the Southern Ocean (*11*), expressed in dynamic meters relative to the 1000-dbar level. The dots indicate the locations of six pairs of altimeter crossover clusters (A through F), and the ×'s indicate the locations of two bottom pressure gauges.

the transport of the ACC vary in phase around the Southern Ocean? Answers to these questions can come only from global observing systems. The cost of using a network of ships to observe the ACC for an extended period of time would be prohibitive. One of the most promising means of monitoring ocean circulation over large spatial scales is with a satellite radar altimeter system (*4*).

A radar altimeter measures the altitude of a spacecraft above the sea surface by radio pulse ranging. With an independent knowledge of the height of the spacecraft (the orbit height) referenced to an earth-fixed coordinate system, the height of the sea surface referenced to the same coordinate can be readily obtained. Reviews of the applications of altimetric measurement of the sea surface to the study of ocean currents can be found in the literature (*5*). We present here some results of an attempt to use the data collected by the Seasat altimeter (*6*) to study the large-scale temporal variability of the ACC during the 3-month lifetime of Seasat.

The approach used is a variant of the so-called crossover-difference technique (*7*). A full description of the technique will appear elsewhere (*8*). A crossover difference refers to the difference between the altimeter measurements made at the intersection of an ascending (northbound) and a descending (southbound) ground track. It comprises three components: orbit error, altimeter measurement error, and true sea level variations. With both orbit and altimeter measurement errors properly corrected, the crossover differences have been used to map the mesoscale variability of ocean currents (*7*). However, as far as we know, the information contained in the crossover differences has not yet been exploited to infer the large-scale temporal variability of ocean currents.

Of the various errors contained in the crossover differences, orbit error is by far the most significant. As a first step to reduce orbit error, we applied a crossover adjustment (*9*) to the Seasat geophysical data records (*10*) in overlapping areas of approximately 2500 km by 2500 km around the Southern Ocean between 40°S and 65°S. This procedure reduced the root-mean-square (r.m.s.) crossover difference from 146 to 32 cm. After deleting anomalous values greater than 60 cm, the residual r.m.s. crossover difference was reduced to 24 cm, which was still dominated by residual errors from various sources (orbit, sea-state bias, range delays in the media, and ocean tides). Since the time scales of the errors are generally less than a week whereas those of the large-scale oceanic variability are generally greater than a month, the residual crossover differences can be smoothed over a 20-day window to further reduce the errors. This smoothing procedure reduced the r.m.s. residual crossover difference from 24 to 9 cm with an error of 6 cm (*8*). The resultant smoothed residual crossover differences constitute the data base for the results presented here.

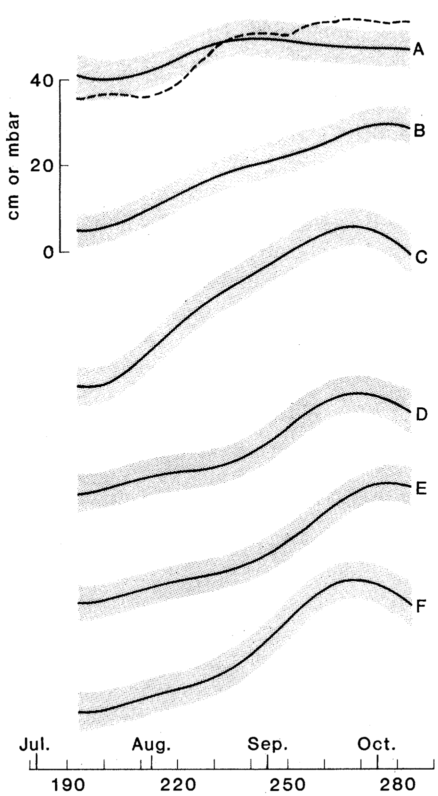

Fig. 2. Time series of the north-south sea level differences (in centimeters) across the six altimeter crossover cluster pairs shown in Fig. 1. The stippled region around each curve represents the r.m.s. error. The dashed line in (A) shows a 20-day running average of the north-south pressure difference (in millibars) across the two bottom pressure gauges (deployed at a depth of 500 m) shown in Fig. 1.

Because of the near-repeat orbit of Seasat, there is a regularly spaced grid of points with a high density of crossovers (referred to here as clusters). We have identified a total of 229 clusters around the ACC, each measuring approximately 200 km by 200 km and containing about 200 crossovers during the 3-month Seasat mission. For each cluster area the crossover adjustment was applied again to remove a constant bias from each track so as to minimize the residual crossover differences. Each resultant bias then effectively represents an along-track average of the time-varying sea level over a distance of ~200 km and hence reflects predominantly the large-scale variability of ocean currents. We thus generated a sea level time series at each cluster by ordering all the resultant biases by their corresponding altimeter overpass times.

To examine the zonal structure of the ACC variability, we have selected six pairs of crossover clusters along the main axis of the flow and computed the sea level difference across the current. The sea level difference between two clusters is proportional to the average surface geostrophic velocity perpendicular to the line segment connecting the two clusters. Displayed in Fig. 1 are the positions of the six pairs of clusters (labeled from A to F) superimposed on a map produced by Gordon *et al.* (*11*) of the long-term averaged sea-surface dynamic height relative to the 1000-dbar level. The dynamic height is proportional to the stream function of the surface geostrophic flow relative to the 1000-dbar level. The directions of this average relative flow are indicated by the arrows on the figure. The two clusters of pair A are in the vicinity of two bottom pressure gauges (denoted by X's on Fig. 1), which were deployed at a depth of 500 m on the continental slope as part of the International Southern Ocean Study (ISOS) program to monitor the variability of the ACC in the Drake Passage (*1*). The sea level difference across pair A will be compared with the pressure difference across the two gauges.

The sampling interval of the sea level time series generated from altimeter crossover differences is irregular as a result of the irregular overpass times of the altimeter. To compute the difference between two time series, we interpolated the time series to a common time grid at daily intervals, using the optimal interpolation scheme discussed by Bretherton *et al.* (*12*). The resultant sea level differences across the six cluster pairs (northern cluster minus southern cluster) for the period from day 193 (12 July) to day 284 (11 October) of 1978 are shown in Fig. 2. The r.m.s. error is indicated by the stippled region around each curve. A rise in the sea level difference implies an increase in the average surface geostrophic velocity between the two clusters. Because each sea level time series is a solution to a difference equation, there is an arbitrary constant associated with each series. This constant was determined here such that each series started from zero at day 193.

The dashed line superimposed on curve A represents a 20-day running mean of the north-south pressure difference (in millibars) between the two bottom pressure gauges (deployed at a depth of 500 m) in the Drake Passage. If the flow variability in the region were due entirely to barotropic motions, then the two curves would match each other to the extent of measurement errors (*13*). However, the flow variability in the Drake Passage has a substantial baroclinic component (*14*), which can account for part of the discrepancy between the two curves. In fact, the discrepancy found here is due primarily to the difference between sea level and bottom pressure at the northern side of the Passage, where the flow variability is known to be higher. Nevertheless, the general increase in the pressure difference (about 20 mbar) across the Drake Passage indeed has a counterpart in the sea level difference measured by the altimeter (about 10 cm).

Figure 2 shows that there is some zonal coherence in the increase in the sea level difference across the ACC during the Seasat mission. The net increase in the sea level difference across the other five sections is 20 to 30 cm. This change in sea level slope is indicative of an eastward acceleration of the ACC. The variations of the sea level difference across the ACC do not appear to be exactly in phase around the Southern Ocean. Owing to the limited duration of the time series, however, it is not possible to draw any quantitative conclusions about the coherence and phase characteristics of the variability.

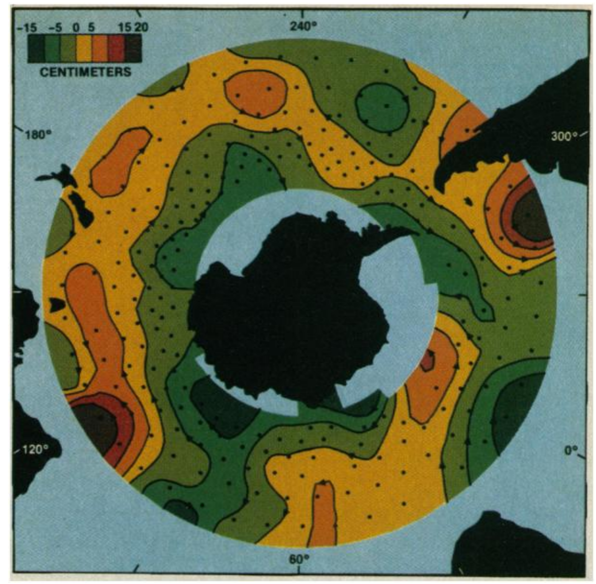

Fig. 3. Color-coded map of the low-frequency (period longer than 20 days) sea level changes measured by the Seasat altimeter over the Southern Ocean between 40°S and 65°S from 12 July to 11 October 1978 (October minus July). The directions of the corresponding change in surface geostrophic velocity are indicated by the arrows. The dots designate the locations of the altimeter measurements used to construct the map.

Figure 3 is a color-coded map showing the net sea level changes (day 284 minus day 193) at the 229 clusters (indicated by dots) around the Southern Ocean (*15*). Because the observed sea level variations are basically characterized by linear trends over the 3-month period (*16*), such a difference map is an effective representation of the variability. The large spatial scales of the variability are clearly evident. During this period, sea level was decreasing over the green areas around Antarctica and increasing over the yellow to brown areas to the north, indicating a general eastward acceleration of the ACC. The directions of the corresponding change in surface geostrophic velocity are indicated by the arrows, showing substantial meridional components in three regions over major topographic features (*17*): 240° to 270°, 330° to 30°, and 60° to 90°. At longitudes 0° and 90° there are exceptions to the generally eastward acceleration. The large, localized increase in sea level southeast of South America and south of Australia is probably due to local phenomena unrelated to the ACC.

To the best of our knowledge, the results presented here provide the first direct observational evidence for zonal coherence in the temporal variability of the ACC. Moreover, they demonstrate that even an altimeter with only 1-m accuracy (for the measurement of the sea-surface height) is able to detect large-scale sea level variability with decimeter magnitudes. The shortness of the Seasat data set allows only a glimpse of a phenomenon whose temporal scales are apparently longer than the 3-month data record. Future altimetric missions such as TOPEX (Ocean Topography Experiment) (*18*), on satellites equipped with improved instruments, hold the promise of providing a more accurate, multiyear view of the large-scale temporal variability of ocean currents such as the ACC.

LEE-LUENG FU

Jet Propulsion Laboratory, California Institute of Technology, Pasadena 91109

DUDLEY B. CHELTON

College of Oceanography, Oregon State University, Corvallis 97331

References and Notes

1. R. B. Wearn, Jr., and D. J. Baker, *Deep-Sea Res.* **27A**, 875 (1980).
2. T. Whitworth III, *J. Phys. Oceanogr.* **13**, 2045 (1983).
3. National Research Council, *Ocean Research for Understanding Climatic Variations* (National Academy Press, Washington, D.C., 1983).
4. W. Munk and C. Wunsch, *Philos. Trans. R. Soc. London Ser. A* **307**, 439 (1982).
5. C. Wunsch and E. M. Gaposchkin, *Rev. Geophys. Space Phys.* **18**, 725 (1980); L.-L. Fu, *ibid.* **21**, 1657 (1983).
6. B. D. Tapley, G. H. Born, M. E. Parke, *J. Geophys. Res.* **87**, 3179 (1982).
7. R. E. Cheney and J. G. Marsh, *Eos (Trans. Am. Geophys. Union)* **62**, 743 (1981); A. L. Gordon *et al.*, *J. Geophys. Res.* **88**, 755 (1983).
8. L.-L. Fu and D. B. Chelton, in preparation.
9. In the crossover adjustment we subtracted a bias from each track such that the crossover differences were minimized in a least-squares sense over a given geographical area. Owing to its large spatial scales (~10,000 km), orbit error can be substantially reduced by this adjustment without compromising oceanic signals.
10. Most of the altimeter measurement errors have been partially corrected for in the data [see (*6*)].
11. A. L. Gordon, E. Molinelli, T. Baker, *J. Geophys. Res.* **83**, 2023 (1978).

12. F. P. Bretherton, R. E. Davis, C. B. Fandry, *Deep-Sea Res.* **23**, 559 (1976).
13. If the density field remains unchanged as for barotropic motions, a change in sea level of 1 cm causes a change in bottom pressure of ~1 mbar.
14. W. D. Nowlin, R. D. Pillsbury, J. Bottero, *Deep-Sea Res.* **28A**, 1 (1981).
15. Before contouring, the data were interpolated to a grid 400 km by 400 km and smoothed over adjacent grid points. The resultant rms error for the map is estimated to be less than 4 cm.
16. The correlation coefficient (sea level versus time) averaged over the 229 clusters (weighted by variance) is 0.7 ± 0.3.
17. See (*11*) for a bathymetry map.
18. The rms accuracy of the TOPEX altimeter is expected to be 14 cm [see TOPEX Science Working Group, *Satellite Altimetric Measurements of the Ocean* (Publication 400-111, Jet Propulsion Laboratory, Pasadena, 1981).
19. We thank M. Parke for useful discussions. The ISOS pressure record used in the study was provided by R. B. Wearn. This research was performed at the Jet Propulsion Laboratory, California Institute of Technology, and at Oregon State University under contract with the National Aeronautics and Space Administration.

20 April 1984; accepted 11 June 1984

Extensive Volcanism Associated with the Separation of Australia and Antarctica

Abstract. *Alternating hard and soft layers characterize the Gull Rock and Tuit Members of the late Eocene Blanche Point Formation, South Australia. Originally the formation was mainly a mixture of volcanic ash, sponge spicules, and calcareous fossil remains, with hard layers produced later by selective silicification. It resembles Cretaceous sediments from western Europe and the eastern coast of the United States, and in each case it appears that alteration of volcanic ash produced smectite and clinoptilolite with release of silica that subsequently crystallized as opal-CT. The occurrence of similar deposits from New Zealand to as far west as Albany, Western Australia, indicates extensive volcanic activity south of Australia in the late Eocene resulting from rifting and separation from Antarctica.*

The Blanche Point Formation consists of about 30 m of fine- to medium-grained sediment deposited in the St. Vincent Basin, South Australia; Reynolds (*1*) described it as a series of hard and soft marls because of the occurrence of numerous, rather regularly silicified, layers within parts of an otherwise weakly lithified claystone. The layers are not entirely coincident with rather indefinite bedding. We consider the origin of the formation as a whole and relate this to regional tectonics, namely, the separation of Australia and New Zealand from Antarctica.

Details of the lithostratigraphy are given in (*2*) and summarized in Fig. 1. Apart from the extra silica in the silicified layers, the rocks consist mainly of calcareous and siliceous fossil fragments with a substantial intermixture of clay minerals ranging in representative samples from 3 to 30 percent. The biogenic component ranges from 25 to 80 percent, quartz from 1 to 13 percent, and coarser, authigenic, generally well crystallized, clinoptilolite, and opal-CT constitute most of the rest (Fig. 2).

The clay minerals, except in the Perkana Member, are mainly smectites containing only 5 to 15 percent interlayered illite (*3*). The Perkana Member also contains kaolinite, which appears to be pseudomorphous after the smectite and formed by alteration of it. Glauconite, much of it pelletal, also occurs throughout the formation but is most abundant in the Tuketja Member. Discrete illite, which may be of detrital terrigenous origin, is minor, and originally the bulk of the clay mineral assemblage throughout the sequence was smectite.

The quartz was initially thought to be of detrital terrigenous origin (Fig. 3, A and B). Although transport in suspension could account for the lack of rounding, the general lack of mosaic texture and the sharp extinction of most grains is evidence of igneous origin. No other primary volcanic component has been recognized.

Sediments formed by diagenetic alteration of vitric ash generally contain smectite, silica minerals, and zeolites. Although the presence of any one of the minerals is not diagnostic, the occurrence of all three in the Blanche Point Formation is strongly suggestive of alteration of volcanic ash. Further, the presence of more than 90 percent essentially pure smectite in the carbonate-free fraction of a sediment of less than 2 μm in diameter appears to be generally accepted as evidence of formation of the smectite by alteration of volcanic ash (*4, 5*). Illite layers comprise less than 15 percent of the predominant smectite of the fraction of less than 2 μm from Blanche Point, supporting a volcanic origin for this component.

Much evidence, including the pristine nature of most of the sponge spicules and the results of chemical mass balance calculations, suggests that silica released by decomposition of original volcanic ash recrystallized as opal-CT. Intensive searching disclosed no evidence of the presence of diatoms or radiolaria.

We conclude that the Blanche Point Formation is of biogenic and volcanic origin, with the formation of the clay minerals and clinoptilolite and the silicification of preferred layers being the result of penecontemporaneous or subsequent diagenetic processes.

Coeval neritic sediments of similar aspect occur sporadically along the southern Australian margin between longitudes 143°30′E and 117°E. In the west, the nonterrigenous portion of the late Eocene Plantagenet Group (*6*) consists mainly of smectite or kaolinite, clinoptilolite, opal-A, and opal-CT; in the east, late Eocene clays at Browns Creek show comparable evidence of volcanic origin. An interval of interlayered tuffs, marls, and spicular marine diatomite beds occurring within the late Eocene Waiareka Volcanic Formation of southern New Zealand at the time shows a direct link between alteration of volcanic sediments and mobilization of silica.

Preservation of such potentially ephemeral neritic ash deposits must demand special conditions: a strong terrigenous input would swamp the ash;

	Member	Lithology		Fossils
BLANCHE POINT FORMATION	Tuit Member	Calcareous, spicular clays and silts; opal-CT layers	Foraminifera and other microfossils	Macrofossils: molluscs, nautiloids and brachiopods, thalassinoid burrows
	Perkana Member	Calcareous clayey spongolite		
	Gull Rock Member	Calcareous, spicular clays and silts; opal-CT layers		Macrofossils: molluscs and nautiloids, thalassinoid burrows
	Tuketja Member	Glauconitic, spicular clayey limestone		Macrofossils: brachiopods

Fig. 1. Stratigraphy of the Blanche Point Formation.